Measurement of matter-antimatter asymmetries with the LHCb experiment

Lukas Bertsch
lukas.bertsch@tu-dortmund.de

Tabea Hacheney
tabea.hacheney@tu-dortmund.de

Tom Troska
tom.troska@tu-dortmund.de

Start of course: 24th of May 2024

TU Dortmund University – Faculty of Physics

Contents

1 Motivation

In our universe, we observe a surplus of particles over antiparticles that is called *baryon asymmetry*. A key aspect in the origin of this matter-antimatter problem is the violation of CP symmetry that occures in weak interactions. In this experiment, the decays of B mesons measured by the LHCb experiment are analyzed to calculate the CP asymmetry in the $B^{\pm} \to h^{\pm}h^{+}h^{-}$

2 Theory

In 1964, CP violation was observed for the first time by Cronin and Fitch [1] in the decay of neutral Kaons. At this time, the Standard Model of particle physics did not provide methods to describe CP violation. This chapter focuses on establishing a connection between the baryon asymmetry and the violation of the CP symmetry. Moreover, the theory behind CP violation is explained.

2.1 Sakharov conditions

For a higher production rate of matter over antimatter, three conditions must be fullfilled. These conditions are referred to as the *Sakharov conditions*, named after the physicist Andrei Sakharov who proposed these criteria in 1966 [2]. First, a violation of the baryon number B is needed. This is in disagreement with the Standard Model as we know it today but extensions of it could allow for baryon number violation.
Second, both the charge symmetry C and the combination of the charge and parity symmetries CP need to be violated. The CP violation is the topic of this lab course and is explained in detail in the following sections.
The third conditon states that the violation of the baryon number (first conditon) needs to occur out of thermal equilibrium. If this was not the true, any baryon number asymmetry would lead to a corresponding reverse process and thus no overall asymmetry could be observed. Consequently, the universe is not in a state of thermal equilibrium.

2.2 *CP* violation in the weak interaction

Before 1970, the weak interaction theory was based on Nicola Cabibbo's notation of the unitary symmetry [3] leading to quark mixing via the Cabibbo angle. This notation described how the weak interaction causes transitions between different quark flavors via

$$u \leftrightarrow d \cdot \cos(\theta_{\mathrm{C}}) \quad \text{and} \quad u \leftrightarrow s \cdot \sin(\theta_{\mathrm{C}}).$$

At this time, only three quarks (u,d,s) were known to be part of the Standard Model. This theory faced issues with renormalizability, failing to adequately describe certain decays or particle interactions. In 1970, Glashow, Iliopoulos, and Maiani proposed a new weak interaction theory [4], introducing a fourth quark (charm) and one vector boson (Z_0). This model helped address these problems and allowed for the integration of the previously predicted boson and the unification with the electroweak interaction. A few years later, in 1973, Kobayashi and Maskawa further refined the theory of the weak interaction by postullating a third generation of quarks [5]. By introducing the quarks now known as *top* and *bottom* quarks, they also extended the theory to a total of three mixing angles θ_i and a *CP* violating phase δ. In summary, the quark mixing matrix is written as

$$\begin{pmatrix} V_{\mathrm{ud}} & V_{\mathrm{us}} & V_{\mathrm{ub}} \\ V_{\mathrm{cd}} & V_{\mathrm{cs}} & V_{\mathrm{cb}} \\ V_{\mathrm{td}} & V_{\mathrm{ts}} & V_{\mathrm{tb}} \end{pmatrix} .$$

This unitary matrix is referred to as the *Cabibbo-Kobayashi-Maskawa* matrix or the *CKM* matrix and can be parameterized in different manners, for example

$$\begin{pmatrix} c_1 & -s_1 c_3 & -s_1 s_3 \\ s_1 c_2 & c_2 c_2 c_3 - s_2 s_3 \mathrm{e}^{\mathrm{i}\delta} & c_1 c_2 s_3 + s_2 c_3 \mathrm{e}^{\mathrm{i}\delta} \\ s_1 s_2 & c_1 s_2 c_3 + c_2 s_3 \mathrm{e}^{\mathrm{i}\delta} & c_1 s_2 s_3 - c_2 c_3 \mathrm{e}^{\mathrm{i}\delta} \end{pmatrix} .$$

Here, s_i and c_i are abbreviations for sines and cosines of the mixing angles θ_i, e.g. $s_1 = \sin\theta_1$. Another representation of the *CKM* matrix is a form with Euler angles, where θ_{12} denotes the Cabibbo angle θ_{C}. The result is

$$\begin{pmatrix} c_{12} c_{13} & s_{12} c_{13} & s_{13} \mathrm{e}^{-\mathrm{i}\delta_{13}} \\ -s_{12} c_{23} - c_{12} s_{23} s_{13} \mathrm{e}^{\mathrm{i}\delta_{13}} & c_{12} c_{23} - s_{12} s_{23} s_{13} \mathrm{e}^{\mathrm{i}\delta_{13}} & s_{23} c_{13} \\ s_{12} s_{23} - c_{12} c_{23} s_{13} \mathrm{e}^{\mathrm{i}\delta_{13}} & -c_{12} s_{23} - s_{12} c_{23} s_{13} \mathrm{e}^{\mathrm{i}\delta_{13}} & c_{23} c_{13} \end{pmatrix} .$$

In another representation of the matrix, the parameters are chosen such that the unity matrix is obtained in the absence of quark mixing. The four degrees of freedom are expressed as

$$\lambda = s_{12} \qquad A = \frac{s_{23}}{s_{12}^2}$$

$$\rho = \Re\left(\frac{s_{13}\mathrm{e}^{-\mathrm{i}\delta}}{s_{12} s_{23}}\right) \qquad \eta = -\Im\left(\frac{s_{13}\mathrm{e}^{-\mathrm{i}\delta}}{s_{12} s_{23}}\right) .$$

Inserting these parameters into the *CKM* matrix leads to an approximation to the order λ^3. It follows that

$$\begin{pmatrix} 1 - \frac{1}{2}\lambda^2 & \lambda & A\lambda^3(\rho - \mathrm{i}\eta) \\ -\lambda & 1 - \frac{1}{2}\lambda^2 & A\lambda^2 \\ A\lambda^3(1 - \rho - \mathrm{i}\eta) & -A\lambda^2 & 1 \end{pmatrix} .$$

In this form, the violation of the *CP* symmetry is found in the parameter ρ and η.

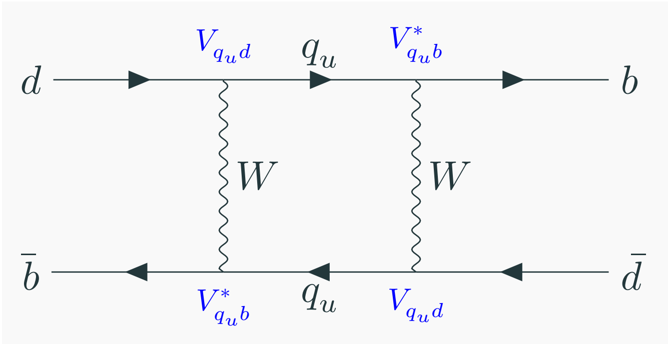

Figure 1: Transition of a B_d^0 meson into a $\bar{B}_d^0$ meson.

2.3 *B* meson decay

The B system is of particular interest for the research of CP violation because of the oscillation of the neutral mesons. Here, B_d^0 mesons oscillate into their antiparticle $\bar{B}_d^0$ and vice versa. The leading order Feynman diagram for this oscillation is depicted in Figure 1.
In the context of this analysis, the CP asymmetry is calculated for the decay of B^+ and B^- mesons. In the absence of CP violation, the production rates of these two mesons are expected to be identical. Hence, a value for the CP violation can be determined by

$$A_{\mathrm{CP}} = \frac{N^+ - N^-}{N^- + N^+}. \tag{1}$$

The number of observed $B^+ \to h^+h^+h^-$ is denoted as N^+, while the matching number of $B^- \to h^+h^-h^-$ is N^-.

3 The LHCb detector

Alongside ALICE, ATLAS and CMS, LHCb is one of the four main experiments located at the Large Hadron Collider (LHC) at CERN. At the LHC, opposing proton beams are brought to collision at the four main interaction points at a rate of 40 MHz. The resulting particle cascades can then be measured and analysed using the different experiments. LHCb is designed to measure decays including b and c quarks which play an important role in the field of CP violation.
The detector is a single-arm forward spectrometer with an acceptance of $2 \leq \eta \leq 5$ in the pseudorapidity range. A schematic view of the apparatus used in the data taking period relevant for this analysis can be seen in Figure 2. The interaction point of the proton-proton collisions is located at the very left where also the Vertex Locator (VELO) is situated. The VELO's primary purpose is to measure the primary and secondary vertices of decays. It therefore needs to provide a high spatial resolution. This information can then be used to reconstruct the lifetime and impact paramter (IP), which is the shortest distance of the primary vetex to the extrapolated particle track. B-mesons, for example,

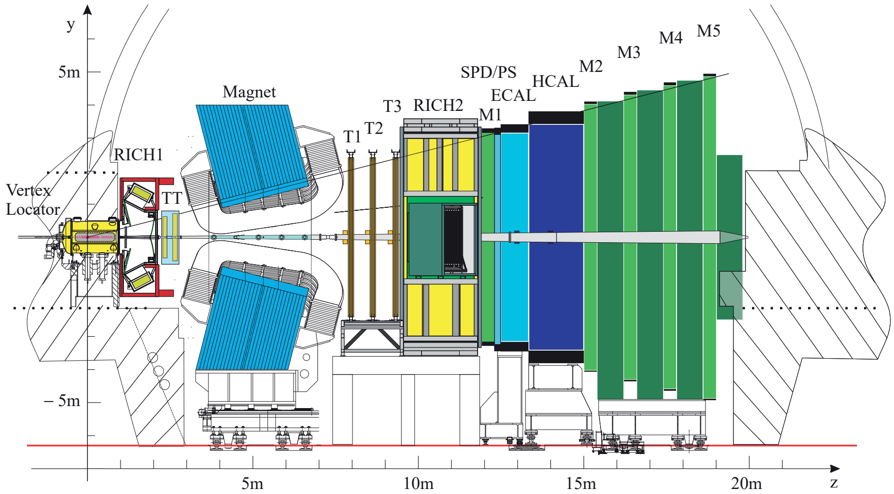

Figure 2: The configuration of the Large Hadron Collider beauty experiment as used in Run 1 [6]. The collision point of the protons is at $z = 0$. The Vertex Locator (VELO), the tracking stations (TT, T1-T3), the Ring Imaging Cherenkov detectors (RICH1-2), as well as the calorimeters (SPD/PS, ECAL, HCAL) and the muon chambers (M1-M5) are shown.

typically decay after a few mm to cm and can therefore be measured in the VELO. The tracking stations TT (Tracker Turicensis) and T1-T3 are used to reconstruct tracks of charged particles deflected by the dipole magnet, which has an integrated field strength of 4 T m. The information from the tracking stations can be used to calculate momentum and charge of a particle. The Ring Imaging Cherenkov detectors RICH 1 and 2 are placed upstream and downstream of the tracking stations, respectively. Here, the velocity of traversing particles is calculated from diameter measurements of light cones caused by the Cherenkov effect. Together with the momentum information, this contributes to the particle identification (PID) and can be used to distinguish kaons from pions. Further downstream, the calorimeter system consisting of the Scintillating Pad Detector (SPD), the Preshower detector (PS) and the electromagnetic- (ECAL) and hadronic (HCAL) calorimeters is located. The calorimeters are utilised to measure the particles energy deposition and also contribute to PID. At the very end of the detector, the muon chambers (M1-M5) measure muons which do not interact much with the aforementioned detector parts.
Events measured by the detector are triggered and preprocessed by a three-level trigger system. The reconstructed decays of interest are then saved for further offline analysis.

4 Analysis strategy

The data used for this analysis was recorded in 2011 at a center of mass energy of 7 TeV. It includes 3.4(5.1) million events of $B^\pm \to h^\pm h^+ h^-$ decays ($h^\pm$: hadron; kaon $K^\pm$/ pion $\pi^\pm$) with dipole magnet polarity up (down), corresponding to an integrated luminosity of

434 pb^{-1} (584 pb^{-1}) [7]. Here, only the decay into three kaons ($h^{\pm} = K^{\pm}$) is considered. A dataset of simulated $B^{\pm} \to K^{\pm}K^{+}K^{-}$ decays is also available. The simulated data are used to understand the signal shape.
First, simulation and real data are compared for relevant observables used in this analysis. Histograms of the distributions of the variables listed in the file are to be created for the simulated and measured data. Next, the energy of the kaons in the simulated data is calculated using the known kaon mass and its momentum. From this, the invariant mass of the B-mesons is calculated. The same is done for the real data after decays with only kaons in the final state are selected using PID information from the variables listed in the dataframe. A high efficiency should be maintained. The differences between the mass distributions of the measured- and simulated data are to be described. Following that, the global CP asymmetry, its uncertainty and significance are calculated. In the next step, Dalitz plots are created for the simulated and real data. Using the Dalitz diagrams, charm resonances that are present in the measured data are identified and removed. Finally, the local CP violation in different areas of the Dalitz plot is to plotted. The areas with the most significant evidence of CP violation are identified and the significance of CP violation in this areas is calculated.

5 Analysis

5.1 Kinematics of the simulated data

To get to know the $B^{\pm} \to K^{\pm}K^{+}K^{-}$ decay, the simulated data is analysed for its kinematic properties. The x, y and z components of the momentum of one of the hadrons are shown in Figure 3. The momenta in the x- and y- direction follow a gaussian distribution. These two axes are perpendicular to the beam. However, the z-component shows negative exponential behaviour.

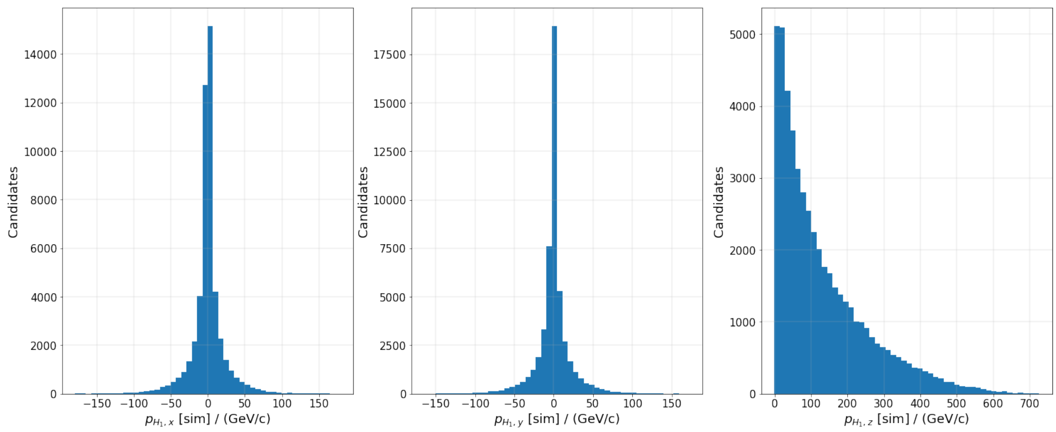

Figure 3: Histograms of the distributions of the momentum vector components for the first hadron of the simulated data.

With these quantities, the magnitude of the momentum is calculated via

$$p = \sqrt{p_x^2 + p_y^2 + p_z^2}. \tag{2}$$

This is done for every kaon candidate and every event. The resulting distribution of the magnitude of the momentum is shown in Figure 4.

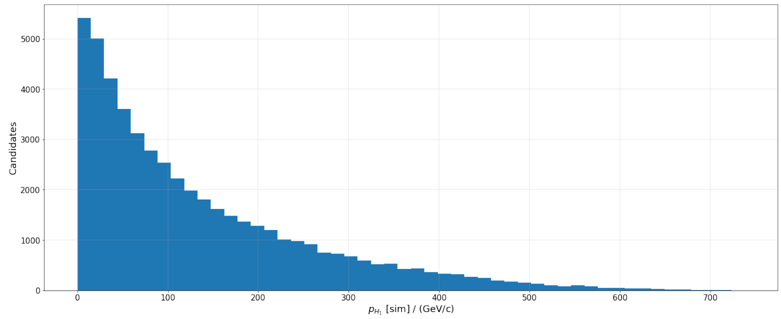

Figure 4: Histogram of the magnitude of the momentum for the first hadron of the simulated data.

By using the relation of energy, mass and momentum given by

$$E^2 = p^2 + m^2, \tag{3}$$

the energy of the hadrons is calculated. The kaon mass is well known and given by $m_{K^\pm} = (493.677 \pm 0.015)\,\text{MeV}$ [8]. The resulting energy distribution of the first hadron is presented in Figure 5.

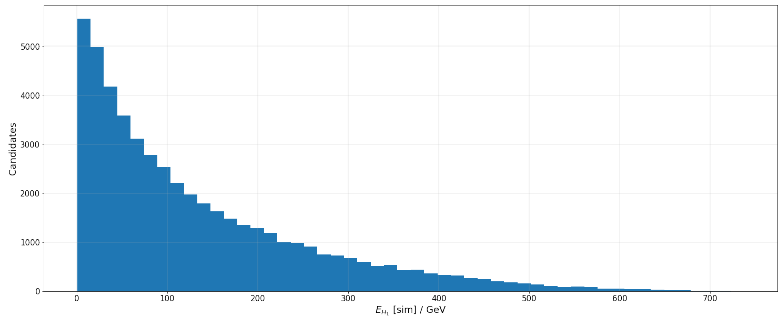

Figure 5: Histogram of the energy of the first hadron of the simulated data.

The energy is also calculated for the other kaon candidates. Since energy and momentum are conserved quantities, the energy and momentum of the $B^\pm$ meson can be calculated using the energy and momentum of the three kaon candidates. The single momentum components of all final state particles are added together and the magnitude of the momentum of the $B^\pm$ meson can be calculated via Equation 2. The energy is calculated by summing the energy of all final state particles. With the energy and the magnitude of

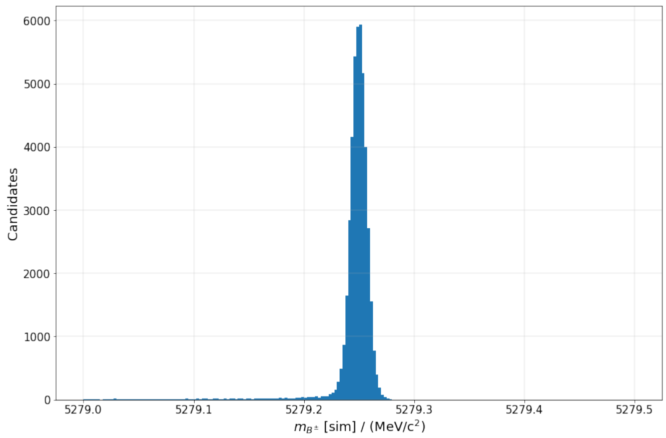

Figure 6: Histogram of the mass of the $B^\pm$ meson of the simulated data.

the momentum, the resulting mass of the $B^\pm$ meson can be calculated via Equation 3. The resulting distribution can be seen in Figure 6. The distribution has a sharp peak at the mass of the $B^\pm$ meson ($m_{B^\pm} = (5279.41 \pm 0.07)\,\mathrm{MeV}$ [8]). This is because the data is simulated data using information about the mass of the $B^\pm$ meson during the simulation process. The distribution for real data would be a lot broader and will also contain combinatorial background.

5.2 Preselection

To reduce combinatorial background and misidentified decays as well as selecting only the decay into kaons one has to apply cuts on parameters describing the likeliness of a final state particle being a kaon, pion or muon. Appropriate requirements are selected using the distributions of the likeliness of the particles being kaons or pions shown in Figure 7. This is done for all three final state hadrons. The cuts are chosen to have a good signal efficiency while also reducing a lot of background. Also, to ensure that the hadrons are not muons, the variable `isMuon` is used for the preselection. The chosen cuts are listed in Table 1.

Preselection			
Variable	Hadron 1	Hadron 2	Hadron 3
`isMuon` (boolean)	is not	is not	is not
`ProbK`	> 0.6	> 0.55	> 0.85
`ProbPi`	< 0.3	< 0.3	< 0.3

Table 1: The chosen cuts for the preselection of the recorded data. The values are chosen according to the distributions shown in Figure 7.

The magnitude of the momentum, the energy as well as the mass of the $B^\pm$ meson is calculated for the real data, just like it has been done in subsection 5.1 for the simulated

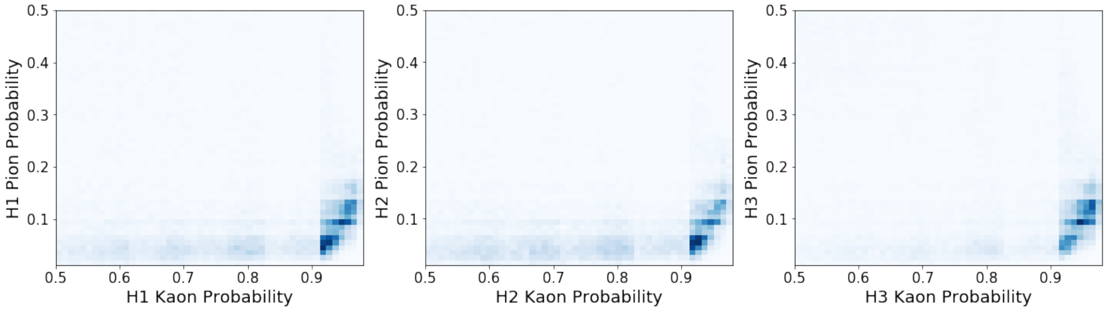

Figure 7: A 2-dimensional histogram for the Kaon and Pion probability of the three hadrons.

data. The resulting distribution of the $B^{\pm}$ meson mass can be seen in Figure 8.

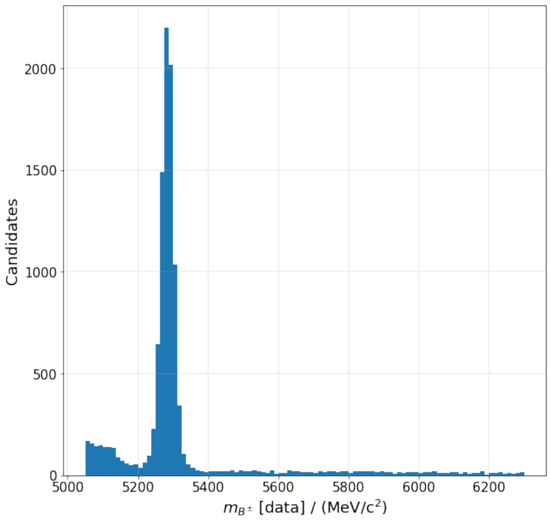

Figure 8: Histogram of the mass of the $B^{\pm}$ meson of the recorded data.

The gaussian distribution of the mass of the $B^{\pm}$ meson for the recorded data is much broader than the one for the simulated data and also contains uniform background as well as more dominant background on the lower end of the invariant mass. To reject the background further, a cut on the $B^{\pm}$ meson mass is applied as $m_B > 5230\,\mathrm{MeV}$ and $m_B < 5370\,\mathrm{MeV}$. Multiple cuts are tested. The chosen cuts seem to be the best choice for rejected most background, while maintaining much signal.

5.3 Global matter anti-matter differences

To study possible *CP* violation, the dataset has to be split for events with $B^+ \to K^+K^+K^-$ and $B^- \to K^-K^+K^-$. The $B^{\pm}$ meson charge is established by looking at the charge of

the kaon candidates. Those events, which have two negatively charged kaons came from a B^- meson and those with two positively charged kaons from a B^+ meson. The raw asymmetry is calculated by summing the number of events in each dataset and using Equation 1.
The resulting raw global asymmetry for the selected events is $A_{CP,\text{raw}} = 0.0427$. In particle physics, a value is only considered an observation, if it is at least five standard deviations. If it exceeds three sigma, it is considered evidence. The uncertainty of the asymmetry can be calculated via

$$\sigma_A = \sqrt{\frac{1 - A_{CP}^2}{N^+ + N^-}}. \tag{4}$$

The significance is the raw asymmetry devided by the resulting uncertainty. The uncertainty for the selected events is $\sigma_{A_\text{raw}} = 0.0110$ and the significance is $S_{A_\text{raw}} = 3.8803$. The raw asymmetry is corrected by the underlying production asymmetry arising from the fact, that the particles are produced by proton-proton collisions. The final asymmetry is calculated by

$$A_{CP} = A_{CP,\text{raw}} - A_{CP,\text{prod}}.$$

The production asymmetry is approximated with 1%. Therefore, the raw statistical uncertainty is not the only uncertainty that should be considered when analysing decays at LHCb. By using Equation 4, the uncertainty for the production asymmetry is $\sigma_{A_{prod}} = 0.0110$. Using gaussian error propagation, the global asymmetry, the final uncertainty, and the significance are

$$\begin{aligned} A_{CP,\text{global}} &= 0.0327 \\ \sigma_{A_{CP,\text{global}}} &= 0.0156 \\ S_{A_{CP,\text{global}}} &= 2.1003. \end{aligned}$$

The result is therefore no longer considered as evidence for an underlying CP asymmetry.

5.4 Dalitz plots and resonances

The decay $B^\pm \to K^\pm K^+ K^-$ does not only occur in the direct way, but also with intermediate R^0 resonances. These resonances are neutral mesons, which then decay into a pair of positively and negatively charged kaons. There are two possible combinations for this, since two kaons always have the same charge. To visualise resonances, a Dalitz plot is drawn. For the Dalitz plot, the masses for these two resonance combinations are calculated just like as for the $B^\pm$ meson. The squared masses of the two resonance combinations are then plotted against each other in a two dimensional diagram. It is important to first look up, which kaon candidates are oppositely charged. In this case, the second and third kaon candidate have the same charge. Therefore, only the combinations R_{12}^0 and R_{13}^0 are neutral, with the indices denoting which final state particles are considered. The combination of the second and third particle would mean, that there was a double positively or negatively charged resonance, which is not possible in the

Standard Model. In this plot, resonances are visible by band structures. Depending on the likeliness of the resonance, these bands can be less or more clear visible.
For the simulated data, the Dalitz plot is shown in Figure 9a. The simulated data does not include resonances and is therefore uniformly distributed. As for the recorded data, the Dalitz plot is shown in Figure 9b.

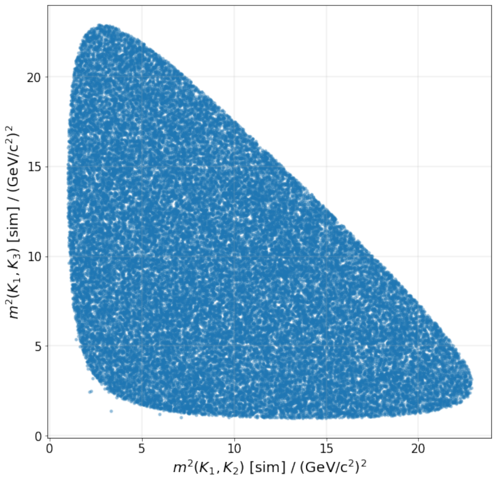

(a) Dalitz plot of the simulated data.

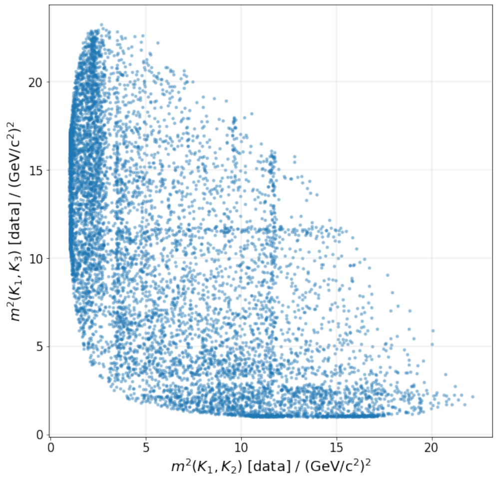

(b) Dalitz plot of the data recorded at the LHCb detector.

Figure 9: Scatter plots of the Dalitz plots for the simulated data and the recorded data.

To make the resonances more visible, it can be helpful to order the resonances R_{12} and R_{13} by mass. This creates a variable "Low", which always includes the resonance with the lower mass and a variable "High" which includes the resonance with the higher mass. The resulting scatter plot is shown in Figure 10a. Also, a binned histogram of the data helps to show higher local densities. This is shown in Figure 10b. Especially Figure 10a shows two main resonances, one being at approximately 3.5 $\frac{\mathrm{GeV}^2}{\mathrm{c}^4}$ and one at approximately 11.5 $\frac{\mathrm{GeV}^2}{\mathrm{c}^4}$. Taking the root of these values gives the mass of the resonances as $R_1^0 \approx 1870\,\frac{\mathrm{MeV}}{\mathrm{c}^2}$ and $R_2^0 \approx 3390\,\frac{\mathrm{MeV}}{\mathrm{c}^2}$. The first resonance R_1^0 as the D^0 meson ($m_{D^0} = (1864.84 \pm 0.05)\,\frac{\mathrm{MeV}}{\mathrm{c}^2}$[8]) and the second resonance R_2^0 as the χ_{c0} meson ($m_{\chi_{c0}} = (3414.71 \pm 0.30)\,\frac{\mathrm{MeV}}{\mathrm{c}^2}$[8]).

5.5 Local matter anti-matter differences

The aim of this analysis is to observe CP violation in charmless $B^{\pm}$ meson decays, cutting out both of the resonances is needed, as they include charm quarks. This is done by excluding the mass ranges

$$1830 - 1890\,\frac{\mathrm{MeV}}{\mathrm{c}^2} \quad \text{and} \quad 3390 - 3440\,\frac{\mathrm{MeV}}{\mathrm{c}^2}$$

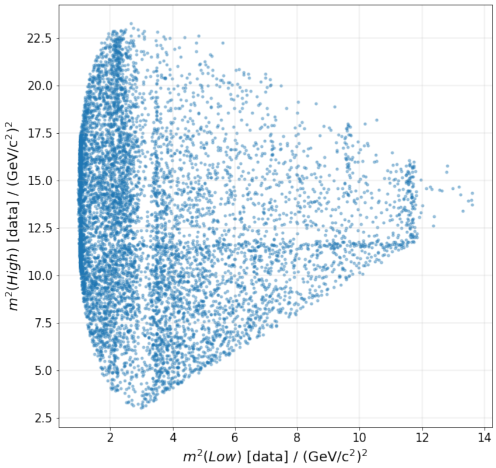

(a) Dalitz plot of the recorded data.

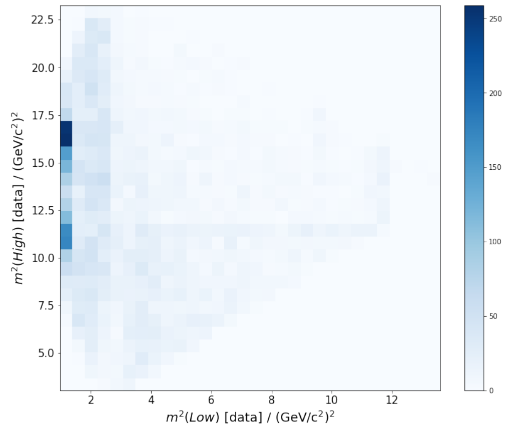

(b) Binned Dalitz plot to visualise local densities.

Figure 10: Two furter visualisations of the Dalitz plot to make resonances better visual.

for both resonances. The Dalitz plot after and before removing the most significant resonances is shown in Figure 11. No clear band structures are visible anymore.

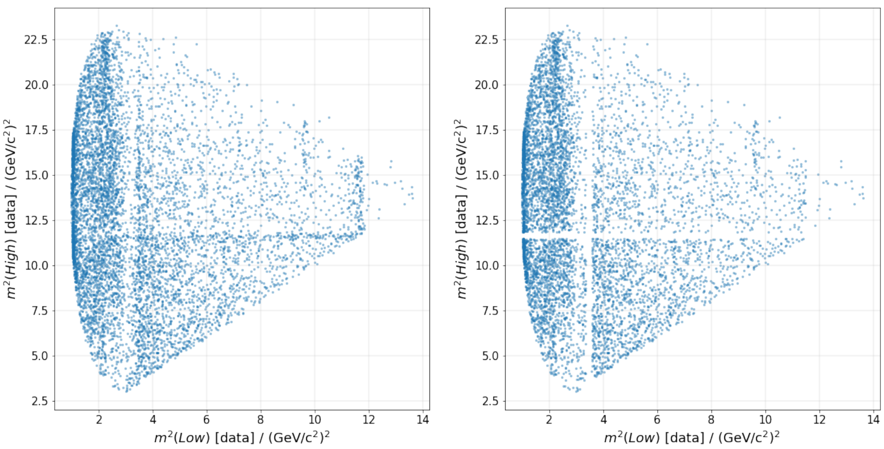

Figure 11: Dalitz plots before (right) and after (left) removing charm resonances.

The *CP* asymmetry is evaluated for different kinematic regions now. To do this, the data is splitted for positively and negatively charged B mesons. The binned dalitz plots for each dataset are shown in Figure 12. The *CP* asymmetry for each bin is shown in Figure 13. The resulting *CP* asymmetry can be misleading, if the statistic in the relative bin is too low. To prevent this and extract a meaningful conclusion, the uncertainty and significance per bin is calculated and shown in Figure 14. As can be seen in Figure 14 and Figure 13, the lower kinematic region shows high significance and asymmetry. This

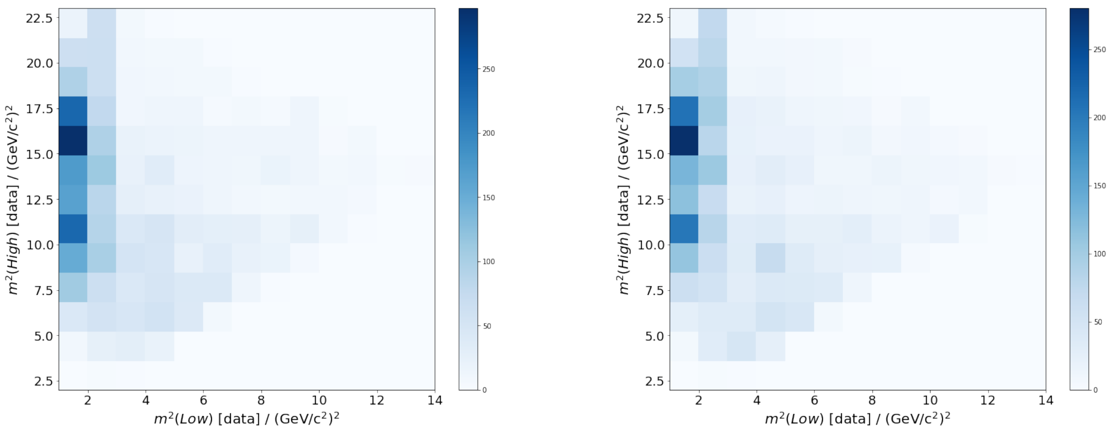

(a) Binned Dalitz plot of the recorded data including only decays of B^+.

(b) Binned Dalitz plot of the recorded data including only decays of B^-.

Figure 12: Binned Dalitz plot to visualise local densities.

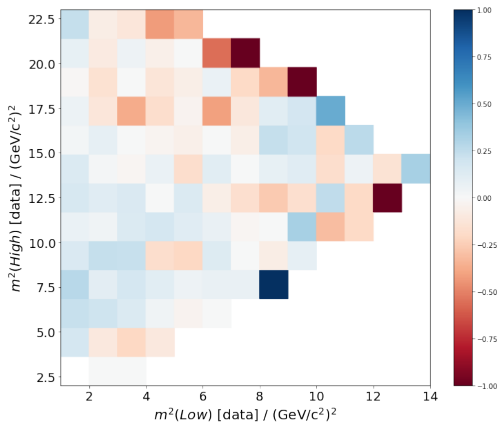

Figure 13: Binned *CP* asymmetry for the recorded data.

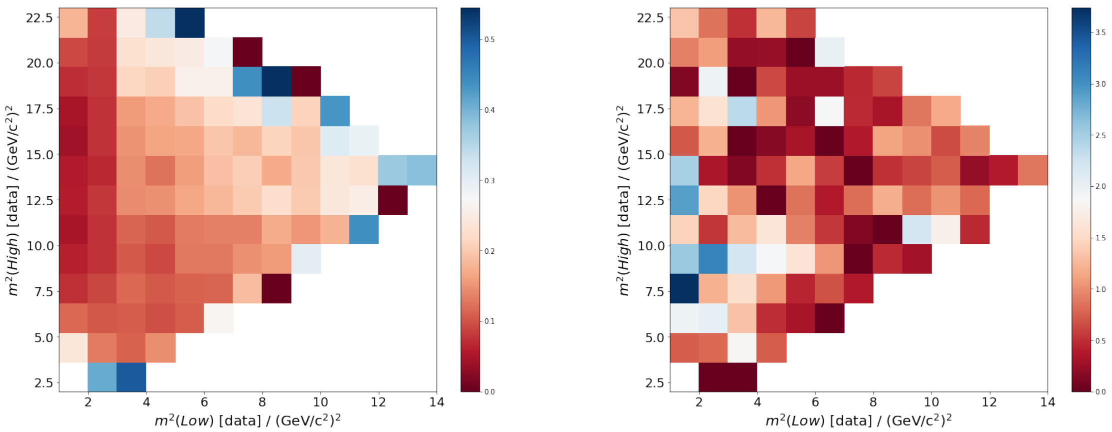

Figure 14: Binned uncertainty (left) and significance (right) for the caluclated CP asymmetry.

region is extracted by applying a cut as

$$m^2_{\text{Low}} < 2\,\frac{\text{GeV}^2}{\text{c}^4} \quad \text{and} \quad m^2_{\text{High}} : 6 - 10\,\frac{\text{GeV}^2}{\text{c}^4} \quad \text{and} \quad 11 - 15\,\frac{\text{GeV}^2}{\text{c}^4}$$

The mass distribution of the B^+ and B^- mesons are shown in Figure 15. The resulting

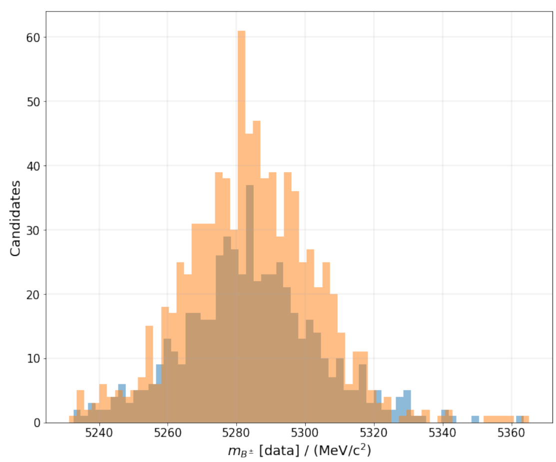

Figure 15: Distributions of the invariant mass of the B^+ (orange) and B^- (blue) candidates in the relevant bins of the Dalitz plot.

local CP asymmetry corrected by the production asymmetry, the overall uncertainty and the significance are

$$\begin{aligned} A_{CP,\text{loc}} &= 0.2245 \\ \sigma_{A_{CP,\text{loc}}} &= 0.0282 \\ S_{A_{CP,\text{loc}}} &= 7.9628. \end{aligned}$$

The found local CP asymmetry can therefore be called a discovery of a local CP asymmetry in $B^{\pm} \to K^{\pm}K^{+}K^{-}$.

6 Discussion

In this analysis, the global CP asymmetry for the decays $B^{\pm} \to K^{\pm}K^{+}K^{-}$ is determined as $A_{CP,\text{global}} = 0.0327 \pm 0.0156$ with a significance of $S_{A_{CP,\text{global}}} = 2.1003$. In the 2013 LHCb analysis on the same data, the global CP asymmetry is determined as

$$A_{CP}(B^{\pm} \to K^{\pm}K^{+}K^{-}) = -0.043 \pm 0.009 \text{ (sys)} \pm 0.003 \text{ (stat)} \pm 0.007(J\Psi K^{\pm})$$

with a significance of 3.7σ [9]. The opposite sign of the asymmetry is due to an opposite definition of the asymmetry observable in Equation 1. Considering the uncertainty of the CP asymmetry determined in this analysis, the values are in agreement with each other. Although systematic uncertainties apart from the estimated production asymmetry are neglected in this analysis but are included in the LHCb analysis, the uncertainties of both values are comparable. This can be explained by the fact, that the analysis here is strongly simplified and selection criteria are not optimised as much as in the LHCb paper and hence rejecting a lot of signal when removing background.
From the Dalitz plots of the two-Kaon masses, resonances at approximately 1870 MeV and 3390 MeV are observed and can be identified with D^0 and χ_{c0} contributions. In the original paper, only the D^0 resonance is accounted for and removed. The strongest local CP asymmetry here is observed in low $m(KK)$ regions which is in agreement to the observations in Ref. [9]. The strongest local CP asymmetry follows as $A_{CP,\text{loc}} = 0.2245 \pm 0.0282$ with a significance of 7.9628σ. In the LHCb analysis, the CP asymmetry in low $m(KK)$ regions reads

$$A^{\text{reg}}_{CP}(B^{\pm} \to K^{\pm}K^{+}K^{-}) = -0.226 \pm 0.020 \text{ (sys)} \pm 0.004 \text{ (stat)} \pm 0.007(J\Psi K^{\pm}) \text{ [9]}.$$

Here, the values are not in agreement, considering the given uncertainties. However, the uncertainty of the value from this analysis is clearly underestimated since no systematic uncertainties are included apart from the estimated production asymmetry of 1 %. Following from that, the claimed significance of 7.9628σ is overestimated. Further, the differences in the observed values could originate from different binning or different mass criteria of the low mass regions as defined in the LHCb paper and here.
All in all, the results achieved in this simplified CP violation analysis are in good agreement with the LHCb observations on the same data. The neglection of systematic uncertainties and different selection criteria can explain the deviations of the observed asymmetries.

References

[1] J. H. Christenson et al. 'Evidence for the 2π Decay of the K_2^0 Meson'. In: *Phys. Rev. Lett.* 13 (4 July 1964), pp. 138–140. DOI: `10.1103/PhysRevLett.13.138`. URL: `https://link.aps.org/doi/10.1103/PhysRevLett.13.138`.

[2] A. D. Sakharov. 'Violation of CP Invariance, C asymmetry, and baryon asymmetry of the universe'. In: *Pisma Zh. Eksp. Teor. Fiz.* 5 (1967), pp. 32–35. DOI: 10.1070/PU1991v034n05ABEH002497.

[3] Nicola Cabibbo. 'Unitary Symmetry and Leptonic Decays'. In: *Phys. Rev. Lett.* 10 (12 June 1963), pp. 531–533. DOI: 10.1103/PhysRevLett.10.531. URL: https://link.aps.org/doi/10.1103/PhysRevLett.10.531.

[4] S. L. Glashow, J. Iliopoulos and L. Maiani. 'Weak Interactions with Lepton-Hadron Symmetry'. In: *Phys. Rev. D* 2 (7 Oct. 1970), pp. 1285–1292. DOI: 10.1103/PhysRevD.2.1285. URL: https://link.aps.org/doi/10.1103/PhysRevD.2.1285.

[5] Makoto Kobayashi and Toshihide Maskawa. 'CP-Violation in the Renormalizable Theory of Weak Interaction'. In: *Progress of Theoretical Physics* 49.2 (Feb. 1973), pp. 652–657. ISSN: 0033-068X. DOI: 10.1143/PTP.49.652. eprint: https://academic.oup.com/ptp/article-pdf/49/2/652/5257692/49-2-652.pdf. URL: https://doi.org/10.1143/PTP.49.652.

[6] A. Augusto Alves Jr. et al. 'The LHCb Detector at the LHC'. In: *JINST* 3 (2008), S08005. DOI: 10.1088/1748-0221/3/08/S08005.

[7] *Measurement of matter-antimatter asymmetries with the LHCb experiment.* TU Dortmund, Faculty of Physics, AG Albrecht. 2022. URL: https://moodle.tu-dortmund.de/pluginfile.php/2306063/mod_resource/content/1/LHCb-CPV.pdf.

[8] *The Review of Particle Physics (2024)*. Particle Data Group. URL: https://pdglive.lbl.gov/Viewer.action (visited on 12/06/2024).

[9] R Aaij et al. 'Measurement of CP violation in the phase space of $B^{\pm} \to K^{\pm}\pi^{+}\pi^{-}$ and $B^{\pm} \to K^{\pm}K^{+}K^{-}$ decays'. In: *Phys. Rev. Lett.* 111 (2013), p. 101801. DOI: 10.1103/PhysRevLett.111.101801. arXiv: 1306.1246 [hep-ex].